ACS APPLIED ELECTRONIC MATERIALS

Open Access

This article is licensed under CC-BY 4.0

pubs.acs.org/acsaelm

Article

Dielectric Properties and Electrical Characteristics of a Triphenylamine Thin Film Deposited onto a Silicon Substrate via Spin Coating

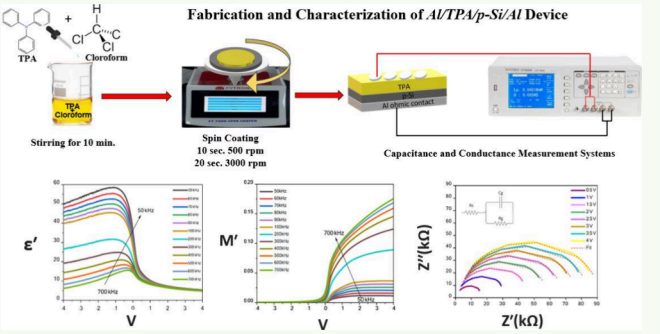
Selcuk Izmirli,* Sukru Cavdar, Orhun Dos, Haluk Koralay, and Nihat Tugluoglu

Cite This: *ACS Appl. Electron. Mater.* 2024, 6, 5057−5066

Read Online

ACCESS | Metrics & More | Article Recommendations

ABSTRACT: This paper presents a complete analysis of the electrical and dielectric attributes of the Al/TPA/p-Si/Al device fabricated by the spin-coating method. In this study, a p-type silicon (p-Si) wafer measuring 1 in. × 1 in. was utilized as the substrate. A layer of organic triphenylamine (TPA) was deposited onto the p-Si wafer. The p-Si wafer itself had a thickness of 525 μm. The TPA layer, serving as the active material, was deposited to a thickness of 170 nm. Additionally, aluminum (Al) contacts were applied to the structure, with a thickness of 150 nm. The primary objective of the current study was to investigate the electrical and dielectric characteristics of the fabricated device, with a specific emphasis on their dependencies on frequency and voltage. The capacitance and conductance of this device were experimentally evaluated at ambient temperature over a frequency spectrum spanning from 50 to 700 kHz. The dielectric variables, including permittivity, dielectric loss, alternating-current conductance, and electrical modulus, were assessed through capacitance and conductance measurements, considering their frequency dependence. Furthermore, the device underwent impedance analysis, allowing for a comprehensive examination and interpretation of its resistive, inductive, and capacitive properties. In consideration of these findings, the goal is to thoroughly investigate the dielectric and electrical characteristics of the Al/TPA/p-Si/Al device. The aim is for an organic-layered device to make significant contributions to the development of electronic devices for diverse applications in the future.



KEYWORDS: *Al/TPA/p-Si/Al, organic-layered diode, thin film, dielectric behaviors, electrical characteristics*

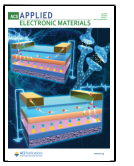
Downloaded via GAZI UNIV on January 9, 2025 at 08:23:32 (UTC).
See https://pubs.acs.org/sharingguidelines for options on how to legitimately share published articles.

1. INTRODUCTION

Semiconductor technology is rapidly advancing, and organic interface metal−semiconductor Schottky diodes play a significant role as circuit elements in various electronic devices.[1−4] Their ability to operate at low voltage levels and exhibit fast-switching capabilities positions them prominently in electronic technology.[5,6] Numerous studies have explored effective device designs, considering variables such as different metal−semiconductor types, manufacturing methods, and material thicknesses.[7] In Schottky diodes, the thin layers formed at the interfaces or in the direction of the rectifier contact significantly influence the electrical properties of the device.[8] These layers can be either organic or inorganic.[9] The preference for semiconductors with organic layers is primarily driven by their cost-effectiveness, ease of application on large surfaces using various coating techniques, and high durability owing to their flexibility.[10−12] Leveraging these fundamental properties, organic semiconductors are extensively employed in electronic and optoelectronic domains, encompassing applications such as organic field-effect transistors, organic light-emitting diodes, solar cells, and Schottky structures.[13−19] Among the organic structures, triphenylamine (TPA; Figure 1) stands out as particularly effective for surface coating in Schottky device designs.[20]

Within the current research inquiry, emphasis is placed on the exploration of dielectric properties and electrical characteristics pertaining to a diode integrated into the Schottky structure denoted as Al/TPA/p-Si/Al. This configuration incorporates an organic layer of TPA. The capacitance−voltage ($C-V$) and conductance−voltage ($G-V$) characteristics were assessed in the absence of light (dark conditions) and at ambient temperature. The measurements were conducted across a frequency range of 50−700 kHz and a voltage range of ±4 V. The influence of frequency and voltage

Received: April 4, 2024
Revised: June 25, 2024
Accepted: June 30, 2024
Published: July 9, 2024



© 2024 The Authors. Published by American Chemical Society

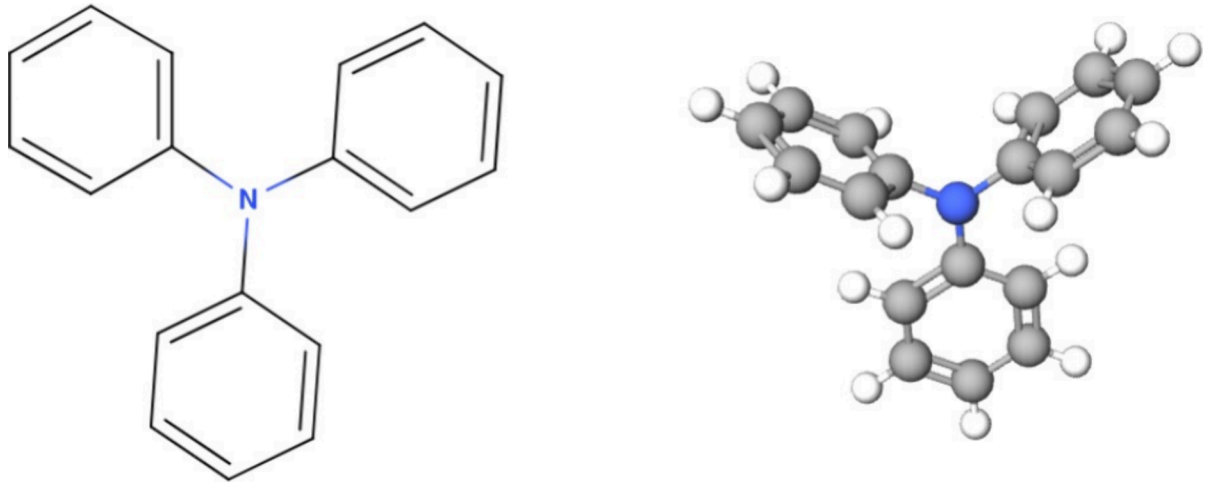


Figure 1. Structure of the compound TPA.

on the dielectric behavior of the Al/TPA/p-Si/Al has been examined and discussed. Additionally, the electrical properties of Al/TPA/p-Si/Al device were examined using impedance and modulus spectroscopy.

2. EXPERIMENTAL SECTION

2.1. Materials. Initial materials were triphenylamine (TPA; Bostonchem %98), aluminum (Al; Heraeus 99%), p-type silicon (p-Si; [100], 1−20 Ω/cm, 525 μm), hydrofluoric acid (HF; Sem Kimya 70%), chloroform ($CHCl_3$; Isolab Chemicals 99.9%), methanol (CH_3OH; Isolab Chemicals 99.9%), acetone [$(CH_3)_2CO$; Isolab Chemicals 99.9%], ultrapure distilled water (UPDW), and nitrogen (N_2; Ankara Gaz 99.9%).

2.2. Fabrication and Characterization of Al/TPA/p-Si/Al Device. In this investigation, a p-Si semiconductor featuring a (100) surface orientation, a resistivity of 1−20 Ω/cm, a thickness of 525 μm, and a polished surface was employed. The p-Si semiconductor underwent chemical cleaning to eliminate both organic and inorganic contaminants from its surface. Subsequently, it underwent ultrasonic cleaning with chloroform, methanol, and acetone, each for 5 min. As a final step, it was treated with hydrofluoric acid for 1 min and thoroughly rinsed with ultrapure water to eliminate the oxide layer.

Immediately following the semiconductor surface cleaning, a layer of elevated purity (99.9%) aluminum, approximately 1500 Å thick, was deposited onto the matte rear surface of the p-Si substrate through thermal evaporation. This process occurred at a pressure of 10^{-6} Torr within a physical evaporation system. In order to attain a low-resistance ohmic contact, the p-Si/Al structure underwent annealing at 575 °C for 5 min in a dry N_2 atmosphere.

For the creation of the organic layer, 0.4 g of TPA was dissolved in 10 mL of chloroform through stirring for 10 min. The resulting TPA organic thin film was deposited onto the shiny surface of the p-Si substrate employing the spin-coating technique, involving spins at 500 rpm for 10 s and 3000 rpm for 20 s. To establish a rectifying contact on the TPA organic layer, aluminum metal with a diameter of 1 mm was deposited using the thermal evaporation method. The TPA layer, serving as the active material, was deposited to a thickness of 170 nm.

Capacitance and conductance measurements were conducted using the Sourcetronic ST2826 LCR Meter characterization system.

3. RESULTS AND DISCUSSION

3.1. Dielectric Studies. To ascertain the dielectric characteristics of the TPA organic semiconductor, we initially conducted assessments of the voltage-dependent variations in capacitance (C) and conductance (G), along with their frequency dependencies, under ambient conditions. Subsequently, at room temperature, we derived the real and imaginary components of the complex dielectric constant (ε' and ε''), the dielectric loss tangent (tan δ), the real and imaginary components of electric modulus (M' and M''), and the alternating-current (AC) electrical conductivity (σ_{ac}) for the Al/TPA/p-Si device in Figure 2. These parameters were extracted from the measured C and G data, considering their dependencies on both frequency and voltage.

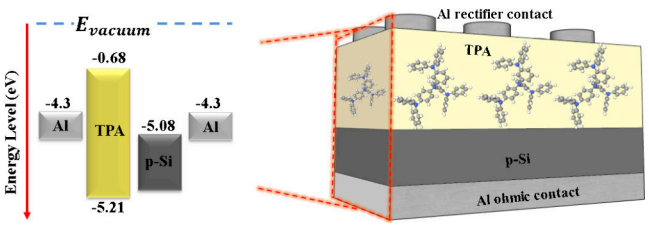


Figure 2. Schematic diagram and energy level of the Al/TPA/p-Si/Al device.

Understanding variations in dielectric parameters concerning voltage and frequency is crucial in diverse domains of electronic and optoelectronic usage areas. Dielectric spectroscopy investigations play a critical role in elucidating the origins and characteristics of dielectric losses. This, in turn, proves valuable for discerning the structural attributes and defects present in solids, encompassing both organic and inorganic structures.

The dielectric constant (ε') and dielectric loss (ε'') of a material delineate the storage and dissipation of energy during each cycle of the applied electric field. This relationship is expressed by eq 1.[21,22]

$$\varepsilon^* = \varepsilon' - j\varepsilon'' \tag{1}$$

The parameter ε' denotes the polarizability and capacitive response of the material, whereas ε'' signifies energy losses attributed to conduction and polarization. The determination of ε' values is conducted within the frequency range of 50−700 kHz at room temperature, employing eq 2[23,24] as follows:

$$\varepsilon' = \frac{C_m d_L}{\varepsilon_0 A} \tag{2}$$

In the given equation, C_m represents the measured capacitance, d_L denotes the thickness of the interfacial organic

https://doi.org/10.1021/acsaelm.4c00600
ACS Appl. Electron. Mater. 2024, 6, 5057−5066

layer, A stands for the rectifier contact area in cm^{-2} of the TPA/p-Si diode, and ε_0 signifies the permittivity of free space ($\varepsilon_0 = 8.85 \times 10^{-12}$ F/m).

Figure 3 illustrates the acquired ε' values as a function of applied voltage for the TPA-based organic layered sample at

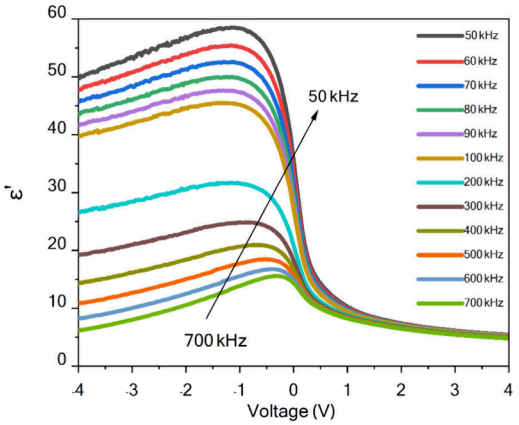


Figure 3. Voltage dependence of the dielectric constant (ε') between 50 and 700 kHz.

selected frequencies (50−700 kHz) under room temperature conditions. Primary objective in this study was to explore the behavior of the prepared sample across a broad range of voltage and frequency, aligning with similar investigations in the literature. In this context, given that the maximum frequency in this study is 700 kHz, we focused on the device's behavior in the accumulation region rather than the depletion region. The value of ε' in the accumulation is approximately 15 at 700 kHz.

The TPA organic interface layer between the Al/p-Si contact exhibited characteristics akin to an insulating layer. Consequently, graphical curves resembling the capacitance behavior of the metal−insulator−semiconductor (MIS) structure were observed in the capacitance graph of the sample. Fundamentally, the capacitance behavior exhibited by the examined structure bears a resemblance to capacitance plots observed in MIS structures.[25] These plots encompass accumulation, depletion, and inversion regions, mirroring the behavior observed in the structure under investigation.

Notably, the plots of ε' for the fabricated device exhibit frequency dispersion, particularly in the negative voltage region. The ε' values exhibit an increasing trend with rising voltage up to 0 V, followed by a subsequent decrease up to 4 V, consistently observed across all frequencies. Additionally, the ε' values demonstrate a pronounced dependence on voltage, with all plots depicting a discernible peak within the voltage range of −0.5 to 0 V.

The observed reduction in ε' values with increasing frequency at each applied voltage is attributed to the presence of interface polarizations. At lower frequencies, the dielectric constant is influenced by both interfacial (space charge) and orientational (dipolar) polarizations. Dipolar and interfacial polarizations exhibit heightened prominence at lower frequencies, where charges within the interface state readily respond to the alternating AC signal, leading to an augmentation in the values of the dielectric constant. In the absence of an electric field, carrier charges bound at different locations or states may manifest diverse dipole orientations. When subjected to an AC field, an electron can transition between two centers, resulting in the reorientation of the electric dipole and subsequent variations in the dielectric constant. Consequently, the observed decrease in frequency and the concurrent increase in the dielectric constant values can be attributed to the influence of dipoles. These findings align reasonably well with similar observations in various materials.[26−31]

The frequency-dependent behavior of ε' at distinct externally applied voltages (−4 to +4 V with intervals of 0.02 V) is investigated for TPA, as illustrated in Figure 4 within

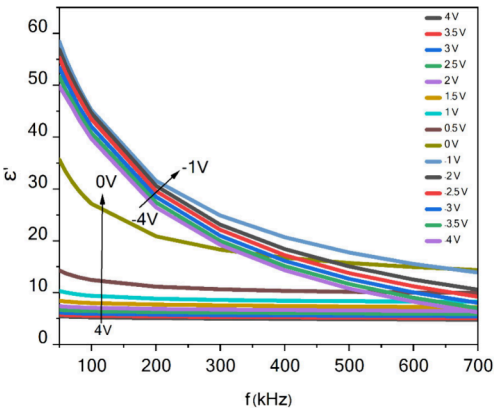


Figure 4. Frequency dependence of the dielectric constant (ε') between −4 and +4 V.

the frequency range of 50−700 kHz. While the distribution of ε' values is more pronounced at positive voltages during low frequencies, this pattern reverses at high frequencies, where it becomes prominent at negative voltages. Additionally, a consistent trend observed across all selected voltage values, both negative and positive, is the decrease in ε' values attributed to the increase in high-frequency values. This observation indicates the presence of interface polarizations in the fabricated device.

The dielectric loss ε'' values were computed based on the measured conductance G_m values, utilizing eq 3.[24,32]

$$\varepsilon'' = \frac{d_L G_m}{A\varepsilon_0 \omega} \tag{3}$$

Here, ω represents the angular frequency. The influence of voltage on ε'' at selected frequencies (50−700 kHz) is investigated for TPA, as illustrated in Figure 5 within the voltage range of −4 to +4 V. Notably, the plots of ε'' for the fabricated device exhibit pronounced frequency dispersion in the negative voltage region. The ε'' values decrease from −4 to +0.5 V with increasing voltage at the specified frequencies. After reaching 0.5 V, ε'' saturates, and there is no further frequency dispersion.

The investigation of the frequency dependence of ε'' was conducted at selected externally applied voltages (−4 to +4 V with intervals of 0.02 V) for TPA, as illustrated in Figure 6 within the frequency range of 50−700 kHz. Notably, the dispersion is more pronounced at lower frequencies. Across all selected voltages, a consistent observation is the decrease in ε''.

It is readily evident that the values of ε'' decrease with increasing frequency. This behavior aligns with the anticipated dielectric response as predicted by space charge and Maxwell−Wagner polarization.[27,33,34] Accordingly, at low frequencies, resistive grain boundaries exert a more pronounced effect compared to conductive grains.[35,36]

https://doi.org/10.1021/acsaelm.4c00600
ACS Appl. Electron. Mater. 2024, 6, 5057−5066

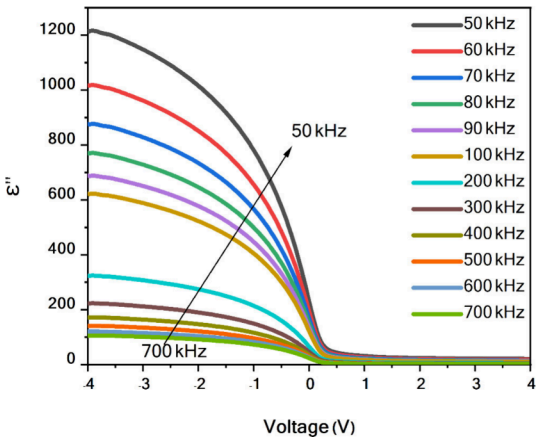


Figure 5. Voltage dependence of the dielectric loss (ε'') between 50 and 700 kHz.

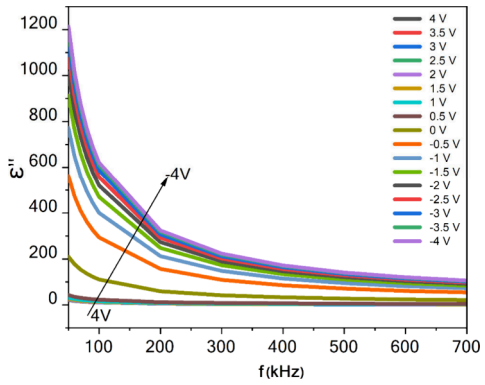


Figure 6. Frequency dependence of the dielectric loss (ε'') between −4 and +4 V.

The observed frequency-dependent variations in ε'' and ε' conform to typical dielectric characteristics. The variation in conductivity with frequency is ascribed to the buildup of charge at the interfaces of less conductive regions, resulting in the emergence of interface polarization and the mechanism of charge hopping.[37−39]

When the electric polarization in a dielectric fails to track the fluctuating electric field, dielectric loss ensues.

The values of the dielectric loss tangent are derived from the calculated ε' and ε'' values, as outlined in eq 4.[29,40] The dissipation factor is commonly referred to as the loss tangent, where the angle δ represents the phase difference between the applied electric field and the induced current.[34]

$$\tan \delta = \frac{\varepsilon''}{\varepsilon'} \tag{4}$$

tan δ values are computed at various voltages and frequencies utilizing eq 4. The voltage and frequency dependencies of tan δ for the TPA/p-Si structure are depicted in Figures 7 and 8, respectively.

As shown in Figure 7, tan δ values exhibit a gradual decrease with increasing frequency. tan δ values below 1 suggest that the displacement current surpasses the conduction current, indicating that the material is most appropriately characterized as a dielectric. Conversely, if the tan δ value exceeds 1, the conduction current predominates, classifying the material as a conductor.[26,29]

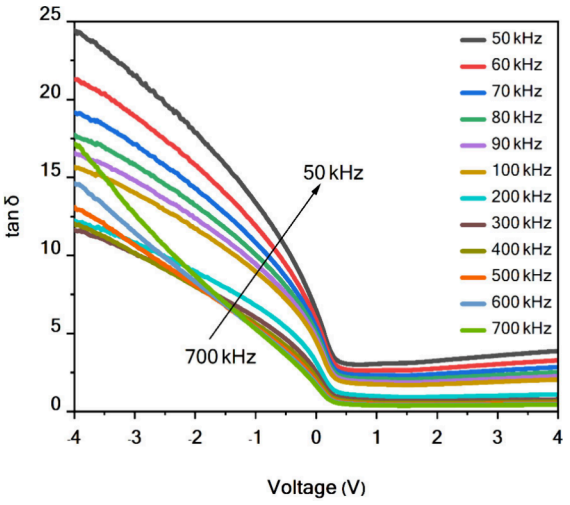


Figure 7. Voltage dependence of tan δ between 50 and 700 kHz.

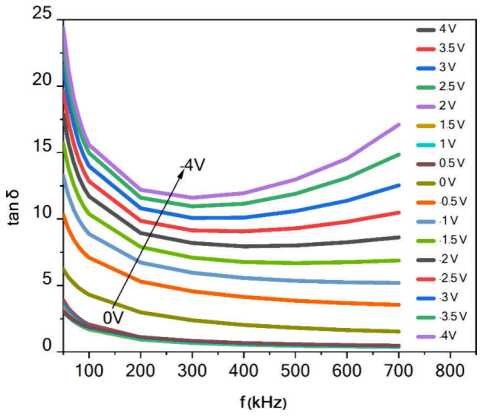


Figure 8. Frequency dependence of tan δ between −4 and +4 V.

As indicated by the tan δ values presented in Figure 7, the TPA/p-Si structure exhibits characteristics akin to a conductor in the negative voltage region. However, in the positive voltage region, the behavior of the structure is predominantly dielectric.

As depicted in Figure 8, the dielectric loss tangent of the fabricated device decreases with increasing frequency in the frequency range of 50−200 kHz, attributed to interface polarization. However, an increase in the loss tangent was observed from 2.5 to 4 V in the high-frequency range of 200−700 kHz. This phenomenon is commonly explained in the literature as dipole polarization relaxation.[41]

The AC electrical conductivity σ_{ac} is a crucial parameter for elucidating the conduction mechanism and identifying the type of carriers responsible for conduction. In the rapidly expanding fields of organic and inorganic electronics and optoelectronics, the AC electrical properties hold substantial importance.[26]

σ_{ac} has been reevaluated solely based on the measured values, utilizing eqs 5 and 6.[24,42,43]

$$\sigma_{ac} = 2\pi f \varepsilon_0 \varepsilon' \tan \delta \tag{5}$$

where f is the applied AC field frequency.

$$\sigma_{ac} = \sigma_{dc} + A\omega^n \tag{6}$$

where σ_{ac} and σ_{dc} are known as the AC and DC conductivity of the device. A and n are designated as the frequency-

https://doi.org/10.1021/acsaelm.4c00600
ACS Appl. Electron. Mater. 2024, 6, 5057−5066

independent preexponential constant and power law exponent, respectively, where $0 < n < 1$. The value of n is 0 for an ideal Debye dielectric dipolar-type material and 1 for an ideal ionic-type material.[43]

Also, the value of DC conductivity (σ_{dc}) can be described by eq 7.

$$\sigma_{dc} = \sum n_i \mu_i q_i \tag{7}$$

where n_i denotes the charge-carrier density, μ_i is the ion mobility, and q_i is the charge of the ion. From eq 7, the enhancement of conductivity can be attributed to changes in both mobility and charge carrier concentration.[44]

As depicted in Figure 9, σ_{ac} decreases up to −0.5 V with increasing voltage at the selected frequencies. Additionally, as

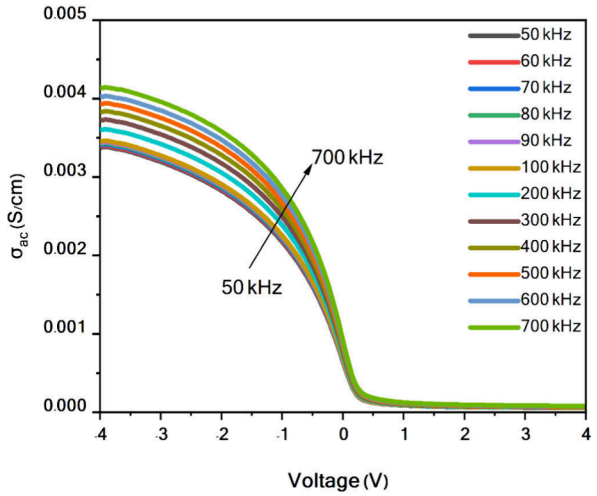


Figure 9. Voltage dependence of σ_{ac} between 50 and 700 kHz.

shown in Figure 8, the σ_{ac} values exhibit an increase with rising frequency. An elevation in σ_{ac} values at high frequencies suggests a decrease in polarization with increasing frequency.[25,45] These σ_{ac} values are contingent solely upon the dielectric loss. These findings align with existing literature, attributing the results to the frequency-dependent behavior of the series resistance (R_s).[25]

As is evident in Figure 10, the σ_{ac} values exhibit two distinct behaviors corresponding to the negative and positive voltage regions. In the negative voltage region, σ_{ac} increases with rising frequency, while in the positive voltage region, it remains nearly constant. Ultimately, the variations in the dielectric parameters and σ_{ac} are attributed to the restructuring and reordering of charges under the influence of an external electric field or voltage at the TPA/p-Si interface, leading to interface polarization.[46]

3.2. Electrical Modulus Studies. To maximize information extraction, dielectric spectroscopy data can be analyzed using electric modulus formalisms introduced by Macedo.[47] Examining the electric modulus as a function of frequency facilitates the identification of relaxation processes within the materials under investigation. Electric modulus analysis is crucial for discerning phenomena such as electrode polarization, grain boundary conduction effects, bulk properties, and electrical conductivity.[48] Moreover, the electric modulus formalism serves as a valuable tool for studying electrical transport mechanisms, including carrier hopping rates and

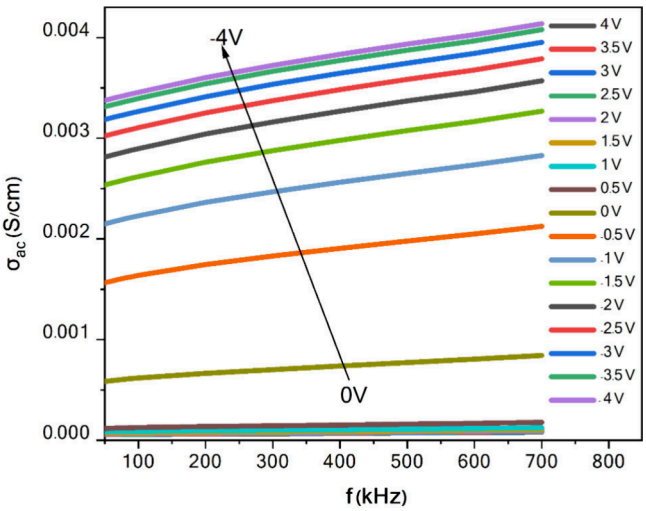


Figure 10. Frequency dependence of the σ_{ac} between −4 and 4 V.

conductivity relaxation phenomena.[49] The electrical modulus M^*, is formulated as per eqs 8 and 9.

$$M^* = \frac{1}{\varepsilon^*} = \frac{1}{\varepsilon' - i\varepsilon''} = \frac{\varepsilon'}{\varepsilon'^2 + \varepsilon''^2} + i\frac{\varepsilon''}{\varepsilon'^2 + j\varepsilon''^2} \tag{8}$$

$$M^* = M' + iM'' \tag{9}$$

M' represents the real part, while M'' denotes the imaginary part of the electrical modulus in the given equations.

Figure 11 illustrates the real component of M^* versus voltage for the TPA/p-Si structure at various frequencies. The

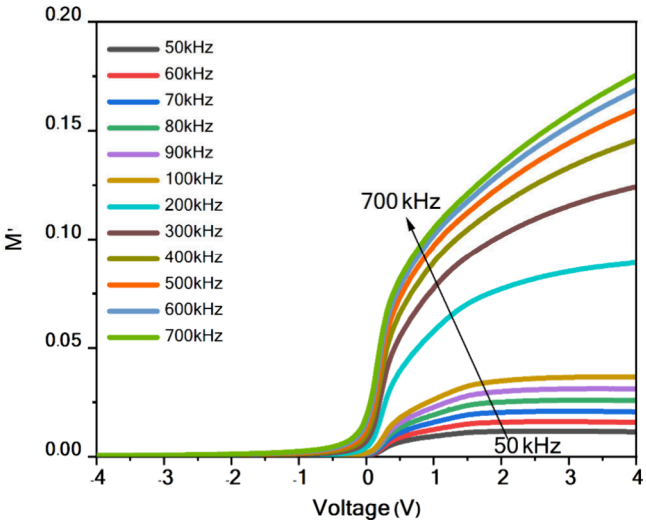


Figure 11. Voltage dependence of the M' between 50 and 700 kHz.

values of M' prove to be highly responsive to the bias voltage, particularly within the depletion zone, exhibiting an increase with ascending frequency, possibly attributed to enhanced polarization at higher frequencies. In Figure 11, there is an exponential growth in M' with increasing voltage at each frequency within the positive voltage region. The M' values reach a maximum at high frequencies and tend toward zero at lower frequencies, indicative of relaxation time effects.

In Figure 12, we have presented a graph depicting the M' against frequency at chosen external voltages. Notably, at a

https://doi.org/10.1021/acsaelm.4c00600
ACS Appl. Electron. Mater. 2024, 6, 5057−5066

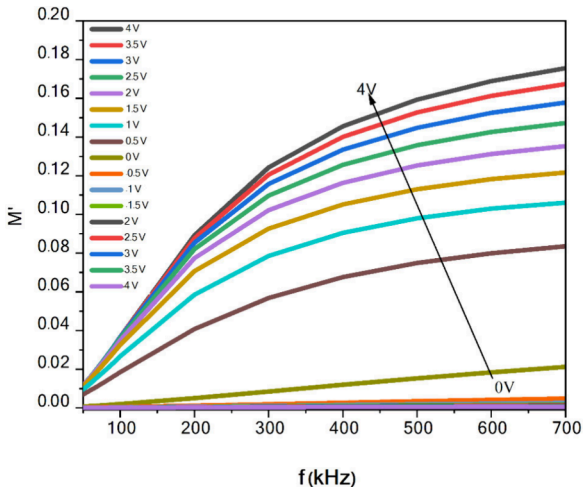


Figure 12. Frequency dependence of the M' between −4 and +4 V.

given frequency, M' exhibits an increment with increasing applied voltage within the positive voltage range. The values of M' remain constant up to a specific frequency threshold, beyond which they exhibit an increase with rising frequency. This variability is attributed to the impact of interface trap levels and lifetimes, responding to the applied frequency through the AC signal.[40,50]

Figure 13 displays the imaginary component of M'' versus voltage for the TPA/p-Si structure at various frequencies.

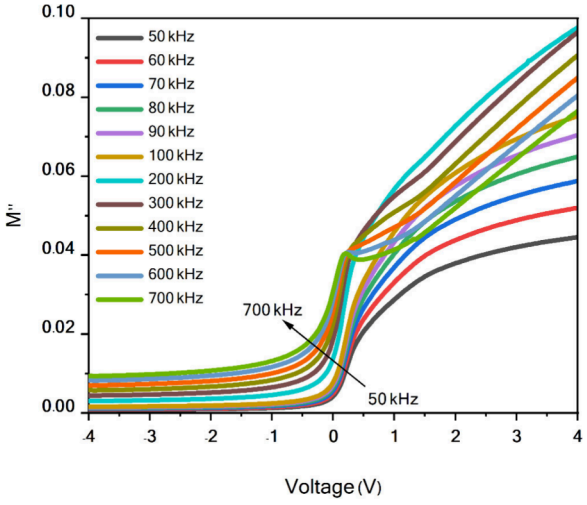


Figure 13. Voltage dependence of the M'' between 50 and 700 kHz.

Analogous to the $M'-V$ plots, frequency dispersion is observable in the $M''-V$ plots, particularly in the forward bias region. Within this region, M'' values rise with increasing frequency. Unlike the $M'-V$ plots, partial dispersion is observed in the negative voltage region in the $M''-V$ plots.

Upon examining Figure 14, it is evident that M'' peaks at all voltage values around a frequency of approximately 200 kHz. This observation suggests that interface states are more influential at lower frequencies, contributing to the observed peaks.[51] No comparable peak has been observed in the literature at negative voltage values.

Upon scrutiny of the Cole−Cole curves in Figure 15, it becomes apparent that the imaginary part of the electrical modulus exerts dominance at frequencies of 50 and 100 kHz.

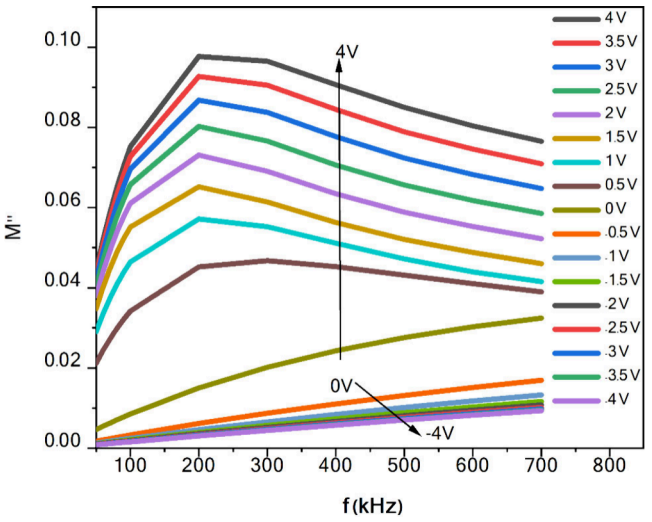


Figure 14. Frequency dependence of the M'' between −4 and +4 V.

However, this effect diminishes at higher frequency values. As depicted in Figure 15, semicircular arcs are discernible in the high-frequency zone, accompanied by reduced impedance values. Consequently, the variation in the Cole−Cole curves of the device signifies the existence of a single relaxation process.[26]

3.3. Impedance Studies. Impedance spectroscopy emerges as a highly effective method for assessing the electrical characteristics of the produced device.[52] This technique enables the calculation and differentiation of contributions from various components, including bulk, electrode, and grain boundaries.[53,54] Consequently, impedance spectroscopy facilitates a comprehensive exploration of the electrical characteristics of a material, providing insights into its various constituents.[55]

Impedance spectroscopy was employed to investigate the AC electrical properties of the nanocomposites. Figures 16 and 17 show Bode magnitude plots of the impedance of the Al/TPA/p-Si/Al device. Figure 16 illustrates the variation in the real part of the complex impedance measurement conducted over a range of voltage values between −4 and +4 V with varying frequencies. The graph reveals that the impedance value of the material remains relatively constant and very close to zero at negative voltage values. In contrast, at positive voltage values, a notable increase in impedance is observed within the low-frequency range, attributed to the elevated voltage levels. This impedance value subsequently decreases as the frequency increases. At higher frequencies, it appears that the real part of the impedance (Z') tends to converge for all nanocomposites, indicating the potential release of space charge.[56]

To evaluate the electrically inhomogeneous nature of the samples, characterized by distinct electro-active regions, the combined imaginary components of impedance and electric modulus plots can be utilized. Figure 17 depicts the changes in the real part of the complex impedance measurement conducted over a range of voltage values between −4 and +4 V at different frequencies. Based on the observation, it is evident that the impedance value of the material remains consistently close to zero at negative voltage values. However, as the voltage becomes positive, the impedance demonstrates an increasing trend correlated with the rise in voltage values, reaching a peak at 200 kHz. The Z'' spectroscopic plot

https://doi.org/10.1021/acsaelm.4c00600
ACS Appl. Electron. Mater. 2024, 6, 5057−5066

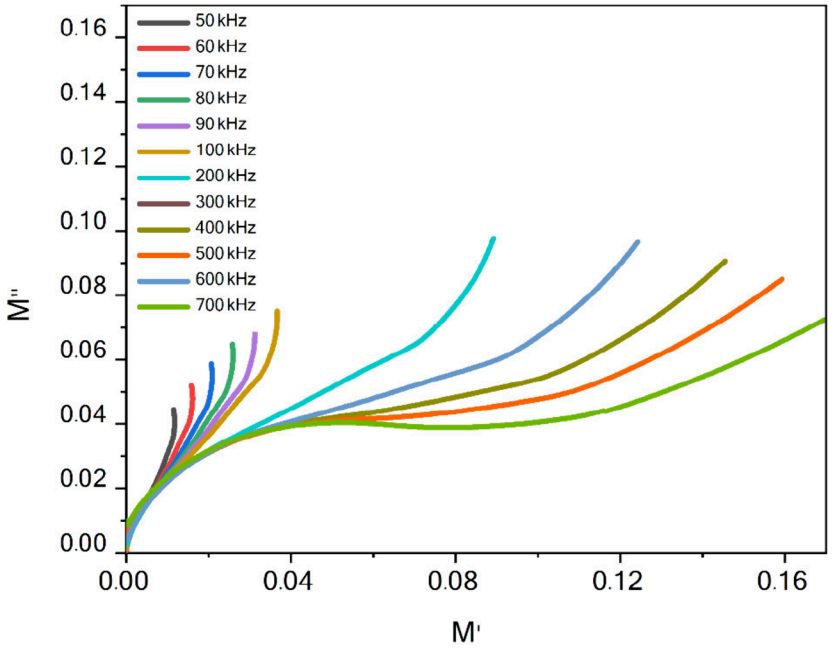


Figure 15. Cole−Cole diagram of M'' vs M' between 50 and 700 kHz.

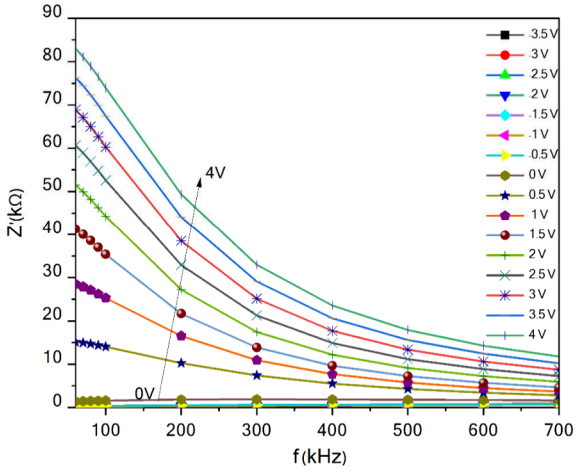


Figure 16. Frequency dependence of Z' between 50 and 700 kHz.

indicates a solitary relaxation event consistently occurring at a frequency of 200 kHz across all positive voltage values examined.[57] Beyond this frequency, the impedance value decreases with the further increase in frequency.

Figure 18 displays representative Nyquist plots of the impedance for the Al/TPA/p-Si/Al device at 300 K and the electrical equivalent circuit of the device. This Nyquist plot illustrates the influence of scanning voltages ranging from 0.5 to 4 V on the charge extraction process. These plots offer insights in the form of arcs or semicircles, with each arc representing an electroactive region characterized by an associated relaxation time ($\tau = RC$), where R denotes the resistance, C signifies the capacitance, and τ represents the relaxation time of the charge carriers.[58] In the low-frequency domain, the concave semicircle delineated along the Z' axis serves as an indicator of the aggregate resistance denoted as R within the sample.[59]

This specific arc characterizes the bulk properties inherent to the sample, while the augmented semicircle conveys information about the grain boundary properties. The magnitude of this arc is indicative of the shunt resistance, and the point of intersection with the Z' axis in the vicinity of the origin defines the series resistance of the device.[60]

Additionally, it was observed that the fitted equivalent circuit for voltages ranging from 0.5 to 4 V comprised the sum of R_s with one-grain resistance (R_g) and grain capacitance (C_g), as depicted in the inset of Figure 18. This circuit encompasses grain resistance and grain capacitance connected in parallel, all linked with series resistance. The Nyquist plots of this device demonstrate the prevalence of resistive effects over capacitive effects on the material's impedance, attributable to the heightened scanning voltage. The impedance spectra performance is defined by the presence of one or more semicircular curves, and their radii depend on the bias voltage, indicating the existence of one relaxation mechanism under the entirely applied voltage. The radius of the semicircle enlarges with an increase in the positive bias, indicating the alteration of the electrical conductivity of the device. This expansion in semicircle radii confirms the modification of the device's electrical conductivity. The magnitude of the semicircle reflects the advancement of electrical charge transmission or recombination at the interface. This is attributed to the interface being the junction point where two different materials with distinct permittivity intersect. Furthermore, it is the site where charge carriers transition and traverse to the opposite side once they attain sufficient energy.[61,62]

In Table 1, it is observed that the resistance values of R_s and R_g increase, while the capacitance value of C_g decreases, in relation to the increase in positive bias voltage values.

4. CONCLUSIONS

In this study, we report the investigation of the dielectric, modulus and impedance characteristics of the Al/TPA/p-Si/Al device were measured in the frequency range of 50−700 kHz at room temperature. The TPA organic semiconductor film was deposited onto a p-type silicon substrate using the spin coating technic. A useful organic−inorganic device was fabricated using TPA. The interfacial states at the metal−

https://doi.org/10.1021/acsaelm.4c00600
ACS Appl. Electron. Mater. 2024, 6, 5057−5066

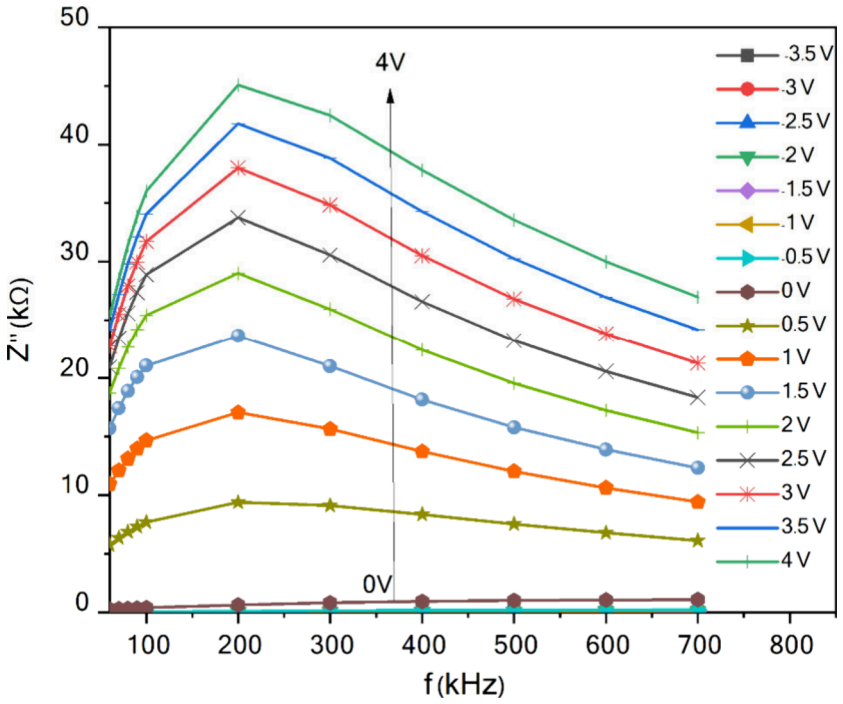


Figure 17. Frequency dependence of Z'' between 50 and 700 kHz.

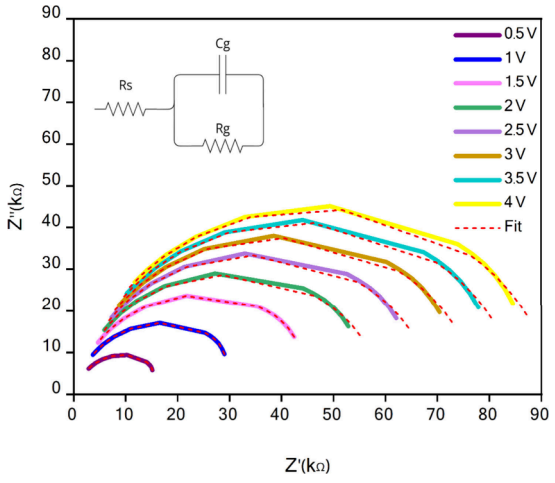


Figure 18. Cole−Cole plots of Z'' vs Z' between 0.5 and 4 V with an equivalent circuit.

Table 1. Fitting Values of R_s, R_g, and C_g

bias voltage (V)	R_s (kΩ)	R_g (kΩ)	C_g (nF)
+4.0	2.580	88.800	8.05
+3.5	2.320	82.300	9.06
+3.0	2.042	74.937	10.3
+2.5	1.742	66.683	12.1
+2.0	1.425	57.349	14.6
+1.5	1.077	46.653	18.2
+1.0	0.536	32.694	23.6
+0.5	0.200	17.644	35.3

semiconductor interface and the organic interface layer played a crucial role in the determination of device characteristics such as dielectric, modulus, and impedance. In the context of dielectric analysis, the decrease in ε' values with the ascending frequency at each applied voltage indicates the presence of interface polarizations. Both interfacial and dipolar polarizations have been identified as influencing the dielectric constant, particularly at lower frequencies. Consistent with analogous studies on diverse materials in existing literature, the concurrent decrease in frequency and rise in ε'' and ε' values are ascribed to the impact of dipoles. Upon analyzing tan δ values, it was discerned that the TPA/p-Si structure manifested properties akin to a conductor in the negative voltage region, whereas its behavior predominantly exhibited dielectric characteristics in the positive voltage region. An augmentation in σ_{ac} values at high frequencies has been noted, attributed to dielectric loss, accompanied by a decline in polarization as the frequency rises. These observations align with the existing literature, attributing the outcomes to the frequency-dependent nature of the series resistance. The frequency-dependent variability of the material, as revealed by modulus analysis, is ascribed to the influence of interface trap levels and lifetimes that respond to the applied frequency through the AC signal. The Nyquist plots generated from the impedance analysis of the device illustrate the predominance of resistive effects over capacitive effects in the material's impedance. Observations reveal that the resistance values of R_s and R_g increase, while the capacitance value of C_g decreases, in relation to the increase in positive bias voltage values. The enlargement in semicircle radii corroborates the alteration in the device's electrical conductivity. The magnitude of the semicircle signifies the progress of electrical charge transmission or recombination at the interface. In conclusion, this study underscores its potential for future technological innovations and contributes scientifically to the comprehension of the dielectric properties and electrical characteristics of the Al/TPA/p-Si/Al structure.

AUTHOR INFORMATION

Corresponding Author

Selcuk Izmirli − *Department of Advanced Technologies, Graduate School of Natural and Applied Sciences, Gazi*

https://doi.org/10.1021/acsaelm.4c00600
ACS Appl. Electron. Mater. 2024, 6, 5057−5066

University, Yenimahalle, Ankara 06500, Turkey; orcid.org/0000-0001-8973-2897; Email: selcuk.izmirli@gazi.edu.tr

Authors

Sukru Cavdar − *Department of Physics, Faculty of Science, Gazi University, Yenimahalle, Ankara 06500, Turkey*

Orhun Dos − *Department of Advanced Technologies, Graduate School of Natural and Applied Sciences, Gazi University, Yenimahalle, Ankara 06500, Turkey; Alparslan Defence Sciences and National Security Institute, National Defence University, Ankara 06400, Turkey*

Haluk Koralay − *Department of Physics, Faculty of Science, Gazi University, Yenimahalle, Ankara 06500, Turkey*

Nihat Tugluoglu − *Department of Energy Systems Engineering, Faculty of Engineering, Giresun University, Giresun 28200, Turkey*

Complete contact information is available at: https://pubs.acs.org/10.1021/acsaelm.4c00600

Author Contributions

The article was written with contributions from all authors. The authors declare that the images and data used in the article belong to this study and approve the final version of the article.

Funding

This work was supported financially by the Gazi University Research Fund (BAP; Grants FDK-2022-7701 and FOA-2022-7389).

Notes

The authors declare no competing financial interest.

REFERENCES

(1) Salem, G. F.; El-Shazly, E. A. A.; Farag, A. A. M.; Yahia, I. S. Spectrophotometric investigations of optical linearity and nonlinearity of pentacene/ITO nanostructure thin film. *Optik* **2018**, *174*, 221−233.

(2) Tombak, A.; Ocak, Y. S.; Asubay, S.; Kilicoglu, T.; Ozkahraman, F. Fabrication and electrical properties of an organic−inorganic device based on Coumarin 30 dye. *Materials science in semiconductor processing* **2014**, *24*, 187−192.

(3) Ulusoy, M.; Altındal, S.; Durmuş, P.; Ozcelik, S.; Azizian-Kalandaragh, K. Frequency and voltage-dependent electrical parameters, interface traps, and series resistance profile of Au/(NiS: PVP)/n-Si structures. *Journal of Materials Science: Materials in Electronics* **2021**, *32* (10), 13693−13707.

(4) Omarbli, S. A.; Gencer Imer, A. Modification in the electronic parameters of M/p-Si hybrid device by PSP functional dye interface with different contact metals (M: Ag, Cu, Pd, Sn). *Synth. Met.* **2023**, *297*, No. 117396.

(5) Zeng, Z.; Li, Z.; Liu, Y.; He, Z.; Jiang, X.; Yu, J.; Wang, J. *2020 IEEE 9th International Power Electronics and Motion Control Conference, IPEMC 2020 ECCE Asia*; Institute of Electrical and Electronics Engineers Inc., 2020; pp 1890−1893.

(6) Umezawa, H.; Shikata, S. I.; Funaki, T. Diamond Schottky barrier diode for high-temperature, high-power, and fast switching applications. *Jpn. J. Appl. Phys.* **2014**, *53* (5S1), No. 05FP06.

(7) Tugluoglu, N. 60Co γ-ray irradiation effects on the interface traps density of tin oxide films of different thicknesses on n-type Si (1 1 1) substrates. *Nuclear Instruments and Methods in Physics Research Section B: Beam Interactions with Materials and Atoms* **2007**, *254* (1), 118−124.

(8) Yahia, I. S.; Zahran, H. Y.; Alamri, F. H.; Aslam Manthrammel, M.; AlFaify, S.; Ali, A. M. Microelectronic properties of the organic Schottky diode with pyronin-Y: Admittance spectroscopy, and negative capacitance. *Physica B: Condensed Matter* **2018**, *543*, 46−53.

(9) Aydin, S. B.; Yildiz, D. E.; Cavus, H. K.; Sahingoz, R. ALD TiO 2 thin film as dielectric for Al/p-Si Schottky diode. *Bulletin of Materials Science* **2014**, *37*, 1563−1568.

(10) Ying, S.; Ma, Z.; Zhou, Z.; Tao, R.; Yan, K.; Xin, M.; Li, Y.; Pan, L.; Shi, Y. Device based on polymer Schottky junctions and their applications: A review. *IEEE Access* **2020**, *8*, 189646−189660.

(11) Zhu, Y.; Song, T.; Zhang, F.; Lee, S. T.; Sun, B. Efficient organic-inorganic hybrid Schottky solar cell: The role of built-in potential. *Appl. Phys. Lett.*, **2013**, *102* (11). DOI: 10.1063/1.4796112

(12) Cavdar, S.; Izmirli, S.; Koralay, H.; Turan, N.; Eymur, S.; Tugluoglu, N. Optoelectronic Properties of Triphenylamine Organic Thin Film Layered Al/p-Si/TPA/Al Heterojunction for Photodiode Application. *ECS Journal of Solid State Science and Technology* **2023**, *12* (4), No. 045001.

(13) Tugluoglu, N.; Calıskan, F.; Yuksel, O. F. Analysis of inhomogeneous barrier and capacitance parameters for Al/rubrene/n-GaAs (100) Schottky diodes. *Synth. Met.* **2015**, *199*, 270−275.

(14) Yoshida, M.; Fujii, A.; Ohmori, Y.; Yoshino, K. Three-layered multicolor organic electroluminescent device. *Appl. Phys. Lett.* **1996**, *69* (6), 734−736.

(15) Suzuki, H.; Hoshino, S. Effects of doping dyes on the electroluminescent characteristics of multilayer organic light-emitting diodes. *J. Appl. Phys.* **1996**, *79* (11), 8816−8822.

(16) Hwang, K.; Yeo, J. S.; Kim, S. S.; Kim, D. Y.; Na, S. I. Efficient organic Schottky junction solar cells with a platinum chloride-treated PEDOT: PSS interfacial layer. *Semicond. Sci. Technol.* **2015**, *30* (1), No. 015014.

(17) Jovanović, D.; Petrović, M.; Tomašević-Ilić, T.; Matković, A.; Bokalič, M.; Spasenović, M.; Rogdakis, K.; Kymakis, E.; Knežević, D.; Cinà, R.; Gajić, R. Long-term stability of graphene/c-Si Schottky-junction solar cells. *Sol. Energy Mater. Sol. Cells* **2023**, *258*, No. 112414.

(18) Yesildag, A.; Erdoğan, M.; Sevgili, O.; Caldıran, Z.; Orak, I. Optical and electrical properties of pyrene−imine organic interface layer based on p-Si. *J. Electron. Mater.* **2021**, *50*, 6448−6458.

(19) Srivastava, A.; Sharma, D.; Srivastava, S. K. Impedance spectroscopy analysis to probe the role of interface properties of surface micro-engineered PEDOT: PSS/n-Si solar cells. *Org. Electron.* **2023**, *119*, No. 106817.

(20) Lian, X.; Zhao, Z.; Cheng, D. Recent progress on triphenylamine materials: synthesis, properties, and applications. *Mol. Cryst. Liq. Cryst.* **2017**, *648* (1), 223−235.

(21) Pissis, P.; Kyritsis, A. Electrical conductivity studies in hydrogels. *Solid State Ionics* **1997**, *97* (1−4), 105−113.

(22) Padma, R.; Sreenu, K.; Rajagopal Reddy, V. Electrical and frequency dependence characteristics of Ti/polyethylene oxide (PEO)/p-type InP organic-inorganic Schottky junction. *J. Alloys Compd.* **2017**, *695*, 2587−2596.

(23) Sharma, M.; Tripathi, S. K. Frequency and voltage dependence of admittance characteristics of Al/Al2O3/PVA: n-ZnSe Schottky barrier diodes. *Materials Science in Semiconductor Processing* **2016**, *41*, 155−161.

(24) Popescu, M.; Bunget, I. *Physics of Solid Dielectrics*; Materials Science Monographs; Elsevier, 1984.

(25) Efil, E.; Kaymak, N.; Seven, E.; Tataroglu, A.; Ocak, S. B.; Orhan, E. Frequency dependent dielectric properties of atomic layer deposition grown zinc-oxide based MIS structure. *Physica B: Condensed Matter* **2019**, *568*, 31−35.

(26) Tugluoglu, N.; Karadeniz, S.; Barıs, B. Electrical modulus and dielectric spectroscopy behavior of spin coated perylene-monoimide semiconductor films. *Materials Science in Semiconductor Processing* **2014**, *27*, 891−898.

(27) Afandiyeva, I. M.; Bulbul, M. M.; Altındal, S.; Bengi, S. Frequency dependent dielectric properties and electrical conductivity of platinum silicide/Si contact structures with diffusion barrier. *Microelectron. Eng.* **2012**, *93*, 50−55.

(28) El-Nahass, M. M.; Metwally, H. S.; El-Sayed, H. E. A.; Hassanien, A. M. Electrical conductivity and dielectric relaxation of

bulk iron (III) chloride tetraphenylporphyrin. *Mater. Chem. Phys.* **2012**, *133* (2−3), 649−654.
(29) Mansour, S. A.; Yahia, I. S.; Yakuphanoglu, F. The electrical conductivity and dielectric properties of CI Basic Violet 10. *Dyes Pigm.* **2010**, *87* (2), 144−148.
(30) Altındal, A.; Coskun, M.; Bekaroglu, O. Dielectric, conduction and interface properties of Au/Pc/p-Si Schottky barrier diode. *Synth. Met.* **2012**, *162* (5−6), 477−482.
(31) Barıs, B. Frequency dependent dielectric properties in Schottky diodes based on rubrene organic semiconductor. *Physica E: Low-dimensional Systems and Nanostructures* **2013**, *54*, 171−176.
(32) Srivastava, S. L.; Dhar, R. Characteristic time of ionic conductance and electrode polarization capacitance in some organic liquids by low frequency dielectric spectroscopy. *Indian Journal of Pure Applied Physics* **1991**, *29* (11), 745−751.
(33) Koops, C. G. On the dispersion of resistivity and dielectric constant of some semiconductors at audiofrequencies. *Phys. Rev.* **1951**, *83* (1), 121.
(34) Shahbazi, M.; Bahari, A.; Ghasemi, S. Structural and frequency-dependent dielectric properties of PVP-SiO2-TMSPM hybrid thin films. *Org. Electron.* **2016**, *32*, 100−108.
(35) Altındal Yeriskin, S.; Erbilen Tanrıkulu, E.; Ulusoy, M. Dielectric properties of MS diodes with Ag: ZnO doped PVP interfacial layer depending on voltage and frequency. *Mater. Chem. Phys.* **2023**, *303*, No. 127788.
(36) Dos, O.; Turan, N.; Tugluoglu, N.; Cavdar, S. The impact of temperature and frequency on negative capacitance and dielectric attributes in NiCo2O4 bulk ceramic. *Ceram. Int.* **2024**, *50* (13), 24487−24498.
(37) Cherif, A.; Jomni, S.; Belgacem, W.; Elghoul, N.; Khirouni, K.; Beji, L. The temperature dependence on the electrical properties of dysprosium oxide deposited on p-Si substrate. *Materials Science in Semiconductor Processing* **2015**, *29*, 143−149.
(38) Fouad, S. S.; Sakr, G. B.; Yahia, I. S.; Abdel-Basset, D. M.; Yakuphanoglu, F. Capacitance and conductance characterization of nano-ZnGa2Te4/n-Si diode. *Mater. Res. Bull.* **2014**, *49*, 369−383.
(39) Kim, J. Y.; Ghajar, A. J. A general heat transfer correlation for non-boiling gas−liquid flow with different flow patterns in horizontal pipes. *International Journal of Multiphase Flow* **2006**, *32* (4), 447−465.
(40) Kar, S.; Narasimhan, R. L. Characteristics of the Si-SiO2 interface states in thin (70−230 Å) oxide structures. *J. Appl. Phys.* **1987**, *61* (12), 5353−5359.
(41) Wang, Z.; Wang, T.; Wang, C.; Xiao, Y. The effect of interfacial interaction-induced soft percolation regime on dielectric properties in Ba(Fe0.5Nb0.5)O3/P(VDF-TrFE) nanocomposites. *J. Mater. Sci.* **2017**, *52* (19), 11496−11505.
(42) Das, S.; Biswal, A. K.; Parida, K.; Choudhary, R. N. P.; Roy, A. Electrical and mechanical behavior of PMN-PT/CNT based polymer composite film for energy harvesting. *Appl. Surf. Sci.* **2018**, *428*, 356−363.
(43) Arya, A.; Sharma, A. L. Structural, electrical properties and dielectric relaxations in Na+-ion-conducting solid polymer electrolytes. *J. Phys.: Condens. Matter* **2018**, *30*, 165402.
(44) Sharma, P.; Kanchan, D. K.; Gondaliya, N. Effect of ethylene carbonate concentration on structural and electrical properties of PEO−PMMA polymer blends. *Ionics* **2013**, *19*, 777−785.
(45) Dubey, A. K.; Singh, P.; Singh, S.; Kumar, D.; Parkash, O. Charge compensation, electrical and dielectric behavior of lanthanum doped CaCu3Ti4O12. *J. Alloys Compd.* **2011**, *509* (9), 3899−3906.
(46) Demirezen, S.; Tanrıkulu, E. E.; Altındal, S. The study on negative dielectric properties of Al/PVA (Zn-doped)/p-Si (MPS) capacitors. *Indian Journal of Physics* **2019**, *93*, 739−747.
(47) Macedo, P. B.; Moynihan, C. T.; Bose, R. The role of ionic diffusion in polarization in vitreous ionic conductors. *Phys. Chem. Glasses* **1972**.
(48) Sutar, B. C.; Choudhary, R. N. P.; Das, P. R. Dielectric and impedance spectroscopy of Sr (Bi0. 5Nb0. 5) O3 ceramics. *Ceram. Int.* **2014**, *40* (6), 7791−7798.
(49) Ayad, M. M.; Zaki, E. A. Synthesis and characterization of polyaniline films using Fenton reagent. *J. Appl. Polym. Sci.* **2008**, *110* (6), 3410−3419.
(50) Coskun, M.; Polat, O.; Coskun, F. M.; Durmus, Z.; Caglar, M.; Turut, A. The electrical modulus and other dielectric properties by the impedance spectroscopy of LaCrO3 and LaCr0.90Ir0.10O3 perovskites. *RSC Adv.* **2018**, *8* (9), 4634−4648.
(51) Yıldız, D. E.; Yıldırım, M.; Gokcen, M. Investigation on dielectric properties of atomic layer deposited Al_2O_3 dielectric films. *Journal of Vacuum Science Technology A* **2014**, *32* (3). DOI: 10.1116/1.4870593
(52) Macdonald, J. R. Impedance spectroscopy and its use in analyzing the steady-state AC response of solid and liquid electrolytes. *Journal of Electroanalytical Chemistry and Interfacial Electrochemistry* **1987**, *223* (1−2), 25−50.
(53) Alivov, Y. I.; Kalinina, E. V.; Cherenkov, A. E.; Look, D. C.; Ataev, B. M.; Omaev, A. K.; Bagnall, D. M.; Chukichev, M. V. Fabrication and characterization of n-ZnO/p-AlGaN heterojunction light-emitting diodes on 6H-SiC substrates. *Appl. Phys. Lett.* **2003**, *83* (23), 4719−4721.
(54) Liu, Y.; Lin, Y. H.; Zhang, B. P.; Nan, C. W.; Li, J. F. High-temperature electrical transport behavior observed in the La1. 96M0. 04CuO4 (M: Mg, Ca, Sr) polycrystalline ceramics. *J. Am. Ceram. Soc.* **2008**, *91* (6), 2055−2058.
(55) Li, M.; Feteira, A.; Sinclair, D. C. Origin of the high permittivity in $(La_{0.4}Ba_{0.4}Ca_{0.2})(Mn_{0.4}Ti_{0.6})O_3$ ceramics. *J. Appl. Phys.* **2005**, *98* (8). DOI: 10.1063/1.2089159
(56) Shah, M.; Sayyad, M. H.; Karimov, K. S.; Maroof-Tahir, M. Investigation of the electrical properties of a surface-type Al/NiPc/Ag Schottky diode using I−V and C−V characteristics. *Physica B: Condensed Matter* **2010**, *405* (4), 1188−1192.
(57) Shah, M.; Khan, N.; Imran, Z.; Khan, M.; Khattak, A.; Khan, A.; Ullah, N. Structural, optical and impedance spectroscopy study of thin film of polyaniline (PANI/ZnO) nanocomposite. *Materials Research Express* **2020**, *7* (1), No. 015314.
(58) Liu, Y.; Cui, T.; Varahramyan, K. All-polymer capacitor fabricated with inkjet printing technique. *Solid-State Electron.* **2003**, *47* (9), 1543−1548.
(59) Paul, G.; Pal, A. J. Impact of band-engineered polymer-interlayers on heterojunction solar cells based on 2D-layered perovskites (Cs3Sb2ClxI9− x). *Sol. Energy* **2022**, *232*, 196−203.
(60) Dasgupta, U.; Chatterjee, S.; Pal, A. J. Thin-film formation of 2D MoS2 and its application as a hole-transport layer in planar perovskite solar cells. *Sol. Energy Mater. Sol. Cells* **2017**, *172*, 353−360.
(61) Ashery, A.; Elnasharty, M. M.; Hameed, T. A. Investigation of electrical and dielectric properties of epitaxially grown Au/n-GaAs/p-Si/Al heterojunction. *Optical Quantum Electronics* **2020**, *52* (11), 490.
(62) Wang, D.; Zhu, J.; Ding, L.; Gao, P.; Pan, X.; Sheng, J.; Ye, J. Interface electric properties of Si/organic hybrid solar cells using impedance spectroscopy analysis. *Jpn. J. Appl. Phys.* **2016**, *55* (5), No. 056601.